Atmos. Chem. Phys. Discuss., 9, 21165–21198, 2009
www.atmos-chem-phys-discuss.net/9/21165/2009/

Atmospheric Chemistry and Physics Discussions

This discussion paper is/has been under review for the journal *Atmospheric Chemistry and Physics (ACP)*. Please refer to the corresponding final paper in *ACP* if available.

Measurements and modelling of molecular iodine emissions, transport and photodestruction in the coastal region around Roscoff

R. J. Leigh[1], S. M. Ball[2], J. Whitehead[4], C. Leblanc[5], A. J. L. Shillings[3], A. S. Mahajan[6], H. Oetjen[6], J. R. Dorsey[4], M. Gallagher[4], R. L. Jones[3], J. M. C. Plane[6], P. Potin[5], and G. McFiggans[4]

[1]Department of Physics and Astronomy, University of Leicester, Leicester, UK.
[2]Department of Chemistry,University of Leicester, Leicester, UK
[3]Department of Chemistry, University of Cambridge, Cambridge, UK
[4]School of Earth, Atmospheric and Environmental Sciences, University of Manchester, Manchester, UK
[5]Station Biologique de Roscoff, UPMC-CNRS, UMR7139, France

[6]School of Chemistry, University of Leeds, Leeds, UK

Received: 11 September 2009 – Accepted: 12 September 2009 – Published: 7 October 2009

Correspondence to: R. J. Leigh (r.j.leigh@leicester.ac.uk)

Published by Copernicus Publications on behalf of the European Geosciences Union.

Abstract

Emissions from the dominant six macroalgal species in the coastal regions around Rosccoff, France, have been modelled to support the Reactive Halogens in the Marine Boundary Layer Experiment (RHaMBLE) campaign undertaken in September 2006. A 2-D model was used to explore the relationship between point and line measurements of molecular iodine concentrations, and total regional emissions, based on seaweed I_2 emission rates measured in the laboratory. The relatively simple modelling technique has produced modelled point and line data, which compare quantitatively with campaign measurements, and provide a link between emission fields and the different measurement geometries used to quantify atmospheric I_2 concentrations during RHaMBLE. During nightime, absolute concentrations in the region of 5 pptv are predicted and measured in the LP-DOAS measurements, with site concentrations predicted and measured up to 40 pptv, compatible with concentrations above Laminariales beds of approximately 2.5 ppbv. Daytime measured concentrations of I_2 at site correlate with modelled production and transport processes, however complete recycling of photodissociated I_2 is required in the model to quantitatively match measured concentrations. Additional local source terms are suggested to provide a feasible mechanism to account for this discrepancy.Total of I_2 emissions over the 100 km^2 region around Roscoff are calculated as 1.5×10^{19} molecules per second during the lowest tides.

1 Introduction

Most techniques for atmospheric composition measurement provide a single point sample, from which conclusions are sought over a given region or scenario. Techniques such as long-path differential optical absorption spectroscopy (LP-DOAS) provide integrated measurements along a folded line of site between a light source and retro-reflector. In many cases, a relatively simple model can significantly improve understanding of the relationship between point and line data, and temporally varying

ACPD

9, 21165–21198, 2009

and spatially inhomogeneous concentrations in a region around the monitoring site. Results are presented here from a model of molecular iodine emissions produced in support of the RHaMBLE campaign hosted at the Station Biologique de Roscoff (SBR) (McFiggans et al., 2009). This model is used to place novel measurements of I_2 from a broad-band cavity ring down system (BBCRDS) and a LP-DOAS instrument into a regional context.

2 The model

The model incorporates two horizontal spatial scales and a temporal domain, with a vertical component included in footprint modelling calculations. The horizontal grid consists of 746 by 227 elements, each of 0.0005×0.0005 degrees extending from −4.2075 to −3.835 degrees longitude, and 48.6725 to 48.7855 degrees latitude. In the Roscoff region, this resolution corresponds to grid boxes of approximately 36.7 m longitudinally by 55.6 m latitudinally. Bathymetry and macroalgal distribution information was mapped on to this model grid. Tide and meterological data was applied to this spatial information at 1-min resolution from 5 to 28 September 2006.

2.1 Seaweed speciation and site bathymetry

The Roscoff inter-tidal zone in front of the SBR extends more than five kilometers in length and about 1 km in width. This very shallow inter-tidal zone at Roscoff means that the waters closest to the shoreline are too shallow for Laminariales species, so although a larger horizontal surface area of seaweed beds becomes exposed at low tide in the vicinity of the SBR, this mainly consists of fucoids. The distribution of seaweed species is rather patchy in the inter-tidal zone and is mainly dominated by *Fucus spp.* and *Ascophyllum* beds, however there is also a small amount of *Laminaria digitata*, *Saccharina latissima* and *Laminaria ochroleuca* in the channel and tide pools between the site and the island Ile de Batz. The south shore of Ile de Batz includes sheltered

shallow patchy habitats with sand and gravel which surround rocky areas covered by fucoids except when exposed to strong tide currents. *L.* (mainly *hyperborea*) beds extend to the north of Ile de Batz, whereas *L. digitata* flourishes in moderately exposed areas or at sites with strong water currents in the western part of the study site (Ile de Batz and islets from Perharidy) and north-east from the Ile de Batz. It also occurs in rockpools up to mid-tide level and higher on wave-exposed coasts of the Ile de Batz.

The vertical zonation of various species of seaweed is very distinct on rocky shores with each species often forming a belt at a certain elevation in the eulittoral zone (the area between the highest and the lowest tides) and also in the subtidal zone (the area extending below the zero of the marine charts). It is thought that the driving force of this zonation is a combination of biotic factors and the tolerance of the different species to abiotic factors such as temperature, light, salinity, dehydration, and mechanical forces caused by wave action (Lüning, 1990). A typical kelp bed from the Roscoff region is shown in Fig. 2. In the North Atlantic, exemplified in the study site in front of the SBR, the eulittoral zone in sheltered habitat is dominated both in coverage and biomass by brown algal species of the order of Fucales (fucoids), such as *Fucus spp.* and *Ascophyllum nodosum*. In addition, species of the order Laminariales (kelps) encompass 4 species which distributed in distinct populations forming belts for the species *L. digitata* in the lowest zone of the eulittoral and upper subtidal, and *L. hyperborea* extending from the upper subtidal to a limit of depth conditioned by the light penetration (about 20 m at Ile de Batz, Table 1). *L. ochroleuca* appears in habitats protected from the dominant wind, mixed with *L. hyperborea* and *Saccharina lattisima* or in monospecific stands, mainly restricted to shallow waters.

Mapping of the seaweed beds in the vicinity of Roscoff has been attempted in two main studies. One in the early 1970s (Braud, 1974) combined aerial photographs and in situ observations obtained from diving and field measurements. The second in the 1990s used both field and airborne spectrometers to map the seaweed and seagrass beds near Roscoff (Bajjouk et al., 1996). The published maps from these previous studies were used to redraw a novel map which was validated by field observations

from September 2006 to September 2009 and superposed with a bathymetry map of the area provided by L. Leveque from the Service Mer et Observation (Roscoff).

The average biomass density in Table 1 were obtained from recent studies on *Ascophyllum nodosum* at Roscoff (Golléty et al., 2008) and *L. digitata* (Gévaert et al., 2008), and from the extensive long-term survey of *L.* populations by Ifremer (Arzel, 1998) using the average biomass of *L. digitata* in September over the last ten years. The average volumic mass of each species was determined experimentally by filling a one-litre volume with seaweed thalli and determining the fresh weight of 5 replicates. The depth limits of the various species at Roscoff were obtained from previous mapping studies and from the Service Mer et Observation, in agreement with published data (Lüning, 1990).

Distributions of *L. digitata*, *L. hyperborea*, *L. ochroleuca*, *Saccharina lattisima*, *Fucus* and *Ascophyllum* are shown in Fig. 1. *Ascophyllum* and *Fucus* beds are inherently mixed, and are mapped together. An assumed mixing ratio of these two species of 65:35 for *Ascophyllum:Fucus* was used for emission modelling.

2.2 Emission rates from exposed macroalgae

Exposure rates for each species of macroalgae were converted into estimated emission rates based on the time since first exposure of each grid square. Emissions in picomoles per minute per gramme fresh weight were taken from Ball et al. (2009) for all species except *L. ochroleuca*, for which measured data were not available, and an assumed emission rate intermediate between *L. digitata* and *Saccharina latissima* was used. All emission rates over time since first exposure are shown in Fig. 3. Emission rates for each species are assumed to be constant after 20 min of continuous exposure. These emission rates were converted into emissions per m^2 using the assumptions shown in Table 1 of mass by species. Emissions each minute were assumed to mix into a layer of 1 m depth, providing a conversion into a volume mixing ratio(VMR). This assumption produces VMRs above hyperborea of approximately 2.5 ppbv.

Actinic fluxes were measured using a Metcon spectral radiometer (Edwards and Monks, 2003), and photolysis frequencies of a number of trace gases calcuated, including molecular iodine (jI_2). The model temporal resolution was matched to the meteorological dataset sampling of 1 min, with the model run in GMT. The model was run on data from 5 to 28 September 2006.

2.3 Footprint analysis

Concentration footprints (as opposed to the more often used flux footprints) were calculated for a range of wind velocities and representative meteorological conditions (determined from the measured data) using the analytical approximation of Schmid (1994). The model is a numerical solution to an analytical approximation of the advection-diffusion equations. While the heterogeneity of the upwind surface makes it rather difficult to draw firm conclusions about the exact form of the concentration footprint, the model is capable of providing sufficiently detailed estimates for the purposes of this simple study. Table 2 shows the range of model input parameters used to provide estimates of the concentration footprint for the range of conditions encountered during the field study period.

The surface roughness lengths used were 0.03 m where the fetch was across the inter-tidal zone. For the water surfaces encountered at high tide, z_0 was determined using the relationship described by Zilitinkevich (1969)

$$z_0 = c_1 \frac{v}{u_*} + \frac{u_*^2}{c_2 g} \quad (1)$$

where u_* is the friction velocity, g the acceleration due to gravity, v is the kinematic viscosity, and c_1 and c_2 are coefficients with highly variable values estimated to be between (for c_1) 0.0–0.48, and (c_2) from ∞ to 81.1. In this study intermediate values of 0.1 and 32.0 were used.

Using this technique, footprints were calculated at 2, 4, 6, 8, and 10 m/s windspeeds, and are shown in Fig. 4. Footprints for different tide heights and wind stengths were

used in the model to characterise anticipated transport of emissions to the site and the LP-DOAS line of sight. Linear interpolations between calculated footprints were used to smooth transitions from each calculated footprint scenario. Wind direction at the site was used to rotate the footprint accordingly. Following scaling and rotation, the footprint for each time step was applyed to the emissions grid to estimate the concentration both at the site, and along the LP-DOAS line of sight. Footprints for the LP-DOAS were obtained through integration along the line of sight, examples of each footprint are shown in Figs. 8 and 9

3 Model results

For each model timestep, the exposed regions of macroalgae were calculated, and emissions estimated based on the length of exposure of each grid cell. The timeseries of temporal input parameters and calculated exposure for each species is shown in Fig. 5. Two example snap-shots of model steps are shown in Figs. 8 and 9. The "curtain" effect during an ebb tide is shown in Fig. 8, as the initial exposure causes a burst of high I_2 emissions. Emissions are lower and more uniform during the flow tide, reflected in the shape of total regional emission curves in Fig. 5.

4 BBCRDS measurements

A broadband cavity ringdown spectrometer was deployed from a shipping container sited on the jetty in front of the SBR, adjacent to the containers housing the campaign's other in situ instruments. Broadband cavity ringdown spectroscopy (BBCRDS) uses light from a pulsed broadband laser to measure the absorption spectrum of samples contained within a high finesse optical cavity (Bitter et al., 2005; Ball and Jones, 2009). In this case, the BBCRDS instrument was configured to detect molecular iodine using several of the I_2 molecule's B←X absorption bands in the wavelength range

560–570 nm. Other atmospheric gases (H_2O, NO_2 and the oxygen dimer O_4) also absorb at these wavelengths and thus contribute to the measured BBCRDS spectra.

The present BBCRDS system is based on an instrument that previously measured I_2 at Mace Head (Ireland) during the 2002 NAMBLEX campaign (Saiz-Lopez et al., 2006) and that was described in detail by Bitter et al. (2005). In the intervening years, the instrument's performance has been enhanced significantly by upgrading several key components, notably a new laser system that yields pulsed broadband light with a factor of two wider bandwidth at green wavelengths, a new clocked CCD camera and improved analysis software/spectral fitting routines. Briefly: a broadband dye laser pumped by a 532 nm Nd:YAG laser (Sirah Cobra and Surelight I-20; 20 Hz repetition rate) generated light pulses with an approximately Gaussian emission spectrum centered at 563 nm (FWHM=5.2 nm). This light was directed into a 187 cm long ringdown cavity formed by two highly reflective mirrors (Los Gatos, peak reflectivity=99.993% at 570 nm). Light exiting the ringdown cavity was collected and conveyed through a 100 μm core diameter fibre optic cable to an imaging spectrograph (Chromex 250is) where it was dispersed in wavelength and imaged onto a clocked CCD camera (XCam CCDRem2). The time evolution of individual ringdown events was recorded simultaneously at 512 different wavelengths, one for each pixel row of the detector, and light from 50 ringdown events was integrated on the CCD camera before storing the data to a computer. Wavelength resolved ringdown times were produced by fitting the ringdown decay in each pixel row (j=1 to 512). The sampled absorption spectrum was then calculated from sets of ringdown times measured when the cavity contained the sample, $\tau(\lambda_j)$, and when flushed with dry nitrogen, $\tau_0(\lambda_j)$:

$$\alpha(\lambda_j)=\frac{R_L}{c}\left(\frac{1}{\tau(\lambda_j)}-\frac{1}{\tau_0(\lambda_j)}\right)=\sum_n \alpha_n(\lambda_j)+\alpha_{\text{con}}(\lambda_j) \quad (2)$$

where c is the speed of light, R_L is the fraction of the cavity that is occupied by absorbing species, $\alpha_n(\lambda_j)$ is the wavelength dependent absorption coefficient of the nth molecular absorber and $\alpha_{\text{con}}(\lambda_j)$ is the absorption coefficient due to all other unstruc-

tured contributions to the spectrum (mainly aerosol extinction). During the first part of the campaign (before 16 September), the cavity was located inside the shipping container and ambient air was drawn into the cavity at 3 l per minute. The cavity was then moved onto the roof of the contrainer and operated in an open-path configuration for the remainder of the campaign. In both cases, appropriate corrections (Shillings, 2009) were made to account for exclusion of the atmospheric sample from the cavitys mirror mounts which were purged with dry nitrogen to prevent contamination of the optical surfaces (i.e. the R_L term in Eq. 2).

BBCRDS absorption spectra were averaged to a time resolution of 5 min and the known absorptions due to ambient H_2O (humidity meter) and O_4 (atmospheric oxygen concentration) were subtracted. The concentrations of I_2 and NO_2 were then retrieved from a multivariate fit of reference absorption cross sections to the structured features remaining in the sample's absorption spectrum using an analysis similar to that developed for differential optical absorption spectroscopy (DOAS) (Platt, 1999; Ball and Jones, 2003; Ball et al., 2009). NO_2 cross sections were taken from Vandaele et al. (1996) and were degraded to the 0.12 nm FWHM instrumental resolution. I_2 cross sections were derived from the PGOPHER spectral simulation program (Western, Access: September 2009; Martin et al., 1986) and were scaled to reproduce the differential cross sections reported by Saiz-Lopez et al. (2004). The top panel of Fig. 7 shows an example BBCRDS spectrum obtained during the campaign, after subtraction of the known absorptions due to H_2O and O_4 and a fitted quadratic function accounting for all unstructured absorptions $\alpha_{\mathrm{con}}(\lambda_j)$. The central and lower panels show respectively the I_2 and NO_2 contributions to the measured absorption overlaid by their fitted reference spectra from the DOAS fitting routine. During the RHaMBLe campaign, the precision of the spectral retrievals was typically 10 pptv for I_2 and 0.2 ppbv for NO_2 (1σ uncertainty, 304 s averaging time). Although not the principal target of this deployment, co-retrieval the NO_2 concentrations served as an important quality assurance parameter with which to monitor the BBCRDS instrument's performance. Throughout the campaign, the NO_2 concentrations measured by BBCRDS were in excellent quantitative agreement with

NO_2 measurements made by the University of York's NOxy chemiluminescence instrument (McFiggans et al., 2009). For example, the gradient of a correlation plot of NO_2 concentrations recorded by the two instruments on 14–15 September was 0.98±0.03.

5 Measurements taken by long path DOAS

During September 2006 the Long Path Differential Optical Absorption Spectroscopy (LP-DOAS) technique (Plane and Saiz-Lopez, 2006) was used to measure the concentrations of I_2, OIO, IO and NO_3. The absorption path extended 3.35 km from the SBR (48.728 latitude, −3.988 longitude), to a small outcrop of the Ile de Batz (48.74 latitude, −4.036 longitude), where a retroreflector array was placed to fold the optical path. The total optical path length was 6.7 km and the beam was 7 to 12 m above the mean sea level. Details of the DOAS instrument employed can be found elsewhere (Mahajan et al., 2009; Saiz-Lopez and Plane, 2004). Briefly, spectra were recorded with 0.25 nm resolution before being converted into differential optical density spectra and the contributions of individual species determined by simultaneous fitting their absorption cross-sections using singular value decomposition (Plane and Saiz-Lopez, 2006). Integrated I_2 concentrations along the line of sight (Saiz-Lopez and Plane, 2004) were retrieved in the 535–575 nm window on a number of days and nights. Results from this instrument are presented comprehensively in Mahajan et al. (2009). Footprints for the LP-DOAS instrument were calculated using the same footprint model, assuming an 8 m path height, integrated and normalised along the line of sight. This provides a modelled integrated measurement which sampled a significant proportion of the region (see Fig. 9. The relationship between regional emissions, maximum above-surface modelled concentrations, and the LP-DOAS measurements is shown in Fig. 6.

5.1 Calculation of total emissions and modelled exposure at the site and along the LP-DOAS line of sight

The total regional emissions were calculated within the model grid for each minute. Site and LP-DOAS footprints were calculated given wind speed, wind direction, and tidal height. The travel time within the footprint was estimated from windspeed, allowing photolytic destruction to be calculated from the travel time of the molecular iodine to the site. Although no chemical modelling was attempted along the lines of Mahajan et al. (2009), a simple recycling parameter was also included in this work, permitting a proportion of photo-dissociated I_2 to be instantly reformed. This recyling was achieved through modification of the photolytic destruction process from

$$I_{2(t)} = I_{2(0)} e^{jI_2 \cdot t} \quad (3)$$

to

$$I_{2(t)} = I_{2(0)} e^{jI_2 \cdot (1-R) \cdot t} \quad (4)$$

Where: $I_{2(t)}$ is the volume mixing ratio of I_2 at time t, $I_{2(0)}$ is the volume mixing ratio of I_2 at time 0 directly above the emission source. jI_2 is the photolysis frequency of I_2 as measured by a spectral radiometer. R is the assumed recycling rate set here to R=0.1, i.e. 10% of the I_2 that is photolysed is reformed by subsequent chemistry (c.f. Mahajan et al., 2009).

Figure 6 shows total calculated regional emissions, the modelled I_2 mixing ratios in air advected to the measurement site (BBCRDS) and the mean I_2 mixing ratio in the air sampled along the LP-DOAS line of sight for three I_2 loss scenarios: (I) no I_2 losses other than dilution as parameterised according to the flux footprint calculation, (II) dilution and irreversible photolytic loss and (III) dilution and photolytic loss less 10% recycling.

6 Comparison of modelled and measured I_2

The full timeseries of modelled data for the BBCRDS and LP-DOAS instruments is shown in Fig. 6. The impact of photolytic destruction during the day is demonstrated by the almost complete removal of I_2 predicted during daylight hours, despite significant emission events.

There were unfortunately very few periods during which the LP-DOAS and BBCRDS systems were both operational on the same day. On 14 September, the LP-DOAS was operational in the morning, and the BBCRDS performed well overnight to the 15 September. Data from these instruments is plotted with model data in Fig. 10. The windspeed on 14 September rose from approximately 0 at midnight (14.0) to 1 ms^{-1} by 14.05 and 3 ms^{-1} by 14.1. The LP-DOAS measurements are in some cases up to four times the modelled concentration, although peak concentrations at the site are modelled to reach the 25 pptv level. The temporal structure of the measured I_2 does correlate with significant emissions and variable meteorological conditions. Similar structures are shown in Figs. 12 and 13 showing data from 5 and 19 September respectively.

Model I_2 concentrations during the day are displayed with photolytic destruction and recycling (at 10%) included (solid lines) and with all destruction processes switched off (dashed lines). The BBCRDS measurements during the morning of the 15 September, shown in Fig. 10 suggest agreement between the model and BBCRDS data, with concentrations at site being significantly more variable than along the averaged LP-DOAS line of sight. This is an expected consequence of the averaging over larger spatial scales of the LP-DOAS technique with respect to the point measurement modelled at site for the BBCRDS instrument. Concentrations at site were both measured and modelled over 40 pptv during nighttime periods. The primary contributions to these concentrations are local emission sources, rather than the larger beds of *L. digitata* and *L. hyperborea*, which remained beyond the site footprint and subject to complete photolytic destruction.

Measurements by the BBCRDS during hours of sunlight on 14 September (Fig. 10) and 10 September (Fig. 11) show significant correlations and magnitude agreement with model predictions with all destruction processes switched off. This is suspected to be a result of local emission sources around the site, which are not included in the existing maps used as model inputs. Such significant reductions in photolytic destruction are not physically reasonable, but are a useful mechanism to explore a combination of alternative explanations including enhanced local emissions, chemical recycling, or a significant alternative source of molecular iodine through recyling or processing of other macroalgal emissions.

Total regional emissions were classified during this measurement period by species, in addition to exposures of LP-DOAS and BBCRDS instruments, providing information on the main contributing species to each measurement technique. Proportions of emissions from each species measured at site, and with the LP-DOAS technique are shown in Table 3. Given that the LP-DOAS line of sight fell directly over a bed of *L. ochroleuca*, the significant contribution of this species to LP-DOAS measurements is expected. Emissions from *L. ochroleuca* are relatively poorly constrained relative to some *L.* species. One potential source of the additional I_2 in the LP-DOAS measurements is therefore provided by an increased emission rate from *L. ochroleuca*, which would impact the LP-DOAS measurements more than the site.

Despite the relative scarcity of *L. digitata* around the measurement site, and under the LP-DOAS line of sight, contributions from this species are significant, while *L. hyperborea* provided over 40% of the total regional emissions and yet consituted less than 0.5% and 2.5% of BBCRDS and LP-DOAS measurements respectively.

7 Conclusions

A simple dynamical model was produced to examine the potential sensitivity of in situ and line of sight measurements based at the Station Biologique de Roscoff to regional emissions of molecular iodine in September 2006. Based on lab measurements of I_2

emissions by species, concentrations above *L. hyperborea* and *L. digitata* beds were predicted at 2.5 ppbv. Total regional emissions for the 100 km^2 zone have been modelled to be up to 1.5× 0^{19} molecules per second during the lowest tides. Modelled concentrations for the LP-DOAS instrument reach a maximum of 30 pptv, and have a similar structure, although lower concentrations compared with measurements. With the significant contribution of *L. ochroleuca* to this measurement, an increase in the stated emission rate from this species provides one potential explanation.

Modelled concentrations at the site are significantly more variable, but can reach up to 80 pptv during major nighttime episodes. Agreement has been demonstrated between the BBCRDS measurements and modelled concentrations around the 20 pptv level. During the day, photolytic destruction should destroy the significant majority of primarily produced I_2 prior to measurement by either technique. There are however significant measured concentrations from the BBCRDS, correlating with modelled structures of I_2 when destruction processes are eliminated, which merit further investigation. Such features may be a result of unmodelled local emissions, a significant missing recycling or source component, or correlated errors in both model and measurement.

Such temporal and spatial analysis is recommended for future measurements in such spatially inhomogeneous and temporal variable emission fields, ideally coupled with a suitable chemistry scheme. When considering concurrent, or almost concurrent measurements of I_2, IO, and particle formation, the rapidly varying meteorology coupled with varying emissions and differing process timescales render more simplistic analyses problematic. Considerations of the rapid destruction processes for I_2, known chemical recycling paths for IO, and the time dependence of observable particle formation in coastal regions is discussed in more detail in McFiggans et al. (2009) and references therein.

Acknowledgements. The authors would like to thank the staff at the Station Biologique de Roscoff for their significant assistance during the RHaMBLE project, and the Natural Environment Research Council for funding the RHaMBLE campaign. Deployment of the BBCRDS instrument to the RHaMBLE campaign was made possible through a grant from the Natural Environment Research Council NE/D00652X/1.

References

Arzel, P.: Les laminaires sur les côtes bretonnes, évolution de l'exploitation et de la flottille de pêche, état actuel et perspectives., Edition de l'Ifremer, p. 139, 1998. 21170

Bajjouk, T., Guillaumont, B., and Populus, J.: Application of Airborne Imaging Spectrometry System Data to Intertidal Seaweed Classification and Mapping, Hydrobiologia, 327, 463–471, 1996. 21169

Ball, S., Hollingsworth, A. M., Humbles, J., Leblanc, C., Potin, P., Langridge, J. M., Lecrane, J.-P., and McFiggans, G.: Spectroscopic Studies of Molecular Iodine Emitted into the Gas Phase by Seaweed., Atmospheric Chemistry and Physics, this issue, XX, 2009. 21170, 21174, 21188

Ball, S. M. and Jones, R.: Broad-band cavity ring-down spectroscopy, Chem Rev., 103, 5239–5262, 2003. 21174

Ball, S. M. and Jones, R.: Broadband Cavity Ring-Down Spectroscopy, in Cavity Ring-Down Spectroscopy: Techniques and Applications, Blackwell Publishing, 2009. 21172

Bitter, M., Ball, S., Povey, I., and Jones, R.: A Broadband Cavity Ringdown Spectrometer for In-Situ Measurements of Atmospheric Trace Gases, Atmos. Chem. Phys., 5, 3491–3532, 2005, http://www.atmos-chem-phys.net/5/3491/2005/. 21172, 21173

Braud, J.-P.: Etude de quelques paramètres écologiques, biologiques et biochimiques chez une phéophycée des côtes bretonnes Laminaria ochroleuca, Revue des Travaux de l'Institut des Pêches Maritimes (ISTPM), 38, 1974. 21169

Edwards, G. D. and Monks, P.: Performance of a single monochromator diode array spectroradiometer for the determination of actinic flux and atmospheric photolysis frequencies, J. Geophys. Res., 108, 8546, doi:10.1029/2002JD002844, 2003. 21171

Gévaert, F., Janquin, M.-A., and Davoult, D.: Biometrics in Laminaria digitata: a useful tool to assess biomass, carbon and nitrogen contents, J. Sea Res., 60, 215–219, 2008. 21170

Golléty, C., Migné, A., and D., D.: Benthic metabolism on a sheltered rocky shore: role of the canopy in the carbon budget, J. Phycol., 44, 1146–1153, 2008. 21170

Lüning, K.: Seaweeds: Their environment, biogeography, and ecophysiology, Wiley, 527 pp., 1990. 21169, 21170

Mahajan, A., Oetjen, H., Saiz-Lopez, A., Lee, J. D., McFiggans, G. B., and Plane, J. M. C.: Reactive iodine species in a semi-polluted environment, Geophys. Res. Lett., 2009GL038018, accepted, 2009. 21175, 21176

Martin, F., Bacis, R., Churassy, S., and Vergès, J.: Laser-induced-fluorescence Fourier transform spectrometry of the $X_1\Sigma_g^+$ state of I_2: Extensive analysis of the $B^3\Pi_u^+ \rightarrow X^1\Sigma_g^+$ fluorescence spectrum of $^{127}I_2$, J. Molec. Spectrosc., 116, 71, 1986. 21174

McFiggans, G., Bale, C. S. E., Ball, S., Beaumes, J. M., Bloss, W. J., Carpenter, L. J., Dorsey, J., Dunk, R., Flynn, M. J., Furneaux, K. L., Gallagher, M. W., Heard, D. E., Hollingsworth, A. M., Hornsby, K. E., Ingham, T., Jones, C. E., Jones, R. L., Kramer, L. K., Langridge, J. M., Leblanc, C., LeCrane, J.-P., Lee, J. D., Leigh, R. J., Longley, I., Mahajan, A. S., Monks, P. S., Oetjen, H., Orr-Ewing, A. J., Plane, J. M. C., Potin, P., Shillings, A. J. L., Thomas, F., von Glasow, R., Wada, R., Whalley, L. K., and Whitehead, J. D.: Iodine-mediated coastal particle formation: an overview of the Reative Halogens in the Marine Boundary Layer (RHaMBLe) Roscoff coastal studey, Atmos. Chem. Phys. Discuss., to be submitted, 2009. 21168, 21175, 21179

Plane, J. M. C. and Saiz-Lopez, A.: Analytical Techniques for Atmospheric Measurement, Blackwell, 510 pp., 2006. 21175

Platt, U.: Modern methods for the measurement of atmospheric trace gases, Phys. Chem. Chem. Phys., 1, 5409–5415, 1999. 21174

Saiz-Lopez, A. and Plane, J. M. C.: Novel iodine chemistry in the marine boundary layer, Geophys. Res. Lett., 31, L04112, doi:10.1029/2003GL019215, 2004. 21175

Saiz-Lopez, A., Saunders, R., Joseph, D. M., Ashworth, S. H., and Plane, J. M. C.: Absolute absorption cross-section and photolysis rate of I2, Atmos. Chem. Phys., 4, 1443–1450, 2004, http://www.atmos-chem-phys.net/4/1443/2004/. 21174

Saiz-Lopez, A., Plane, J. M. C., McFiggans, G., Williams, P. I., Ball, S. M., Bitter, M., Jones, R. L., Hongwei, C., and Hoffmann, T.: Modelling molecular iodine emissions in a coastal marine environment: the link to new particle formation, Atmos. Chem. Phys., 6, 883–895, 2006, http://www.atmos-chem-phys.net/6/883/2006/. 21173

Schmid, H. P.: Source areas for scalars and scalar fluxes, Bound. Lay. Meteorol., 67, 293–318,

1994. 21171
Shillings, A.: Atmospheric Applications of Broadband Cavity Ringdown Spectroscopy, PhD. Thesis, University of Cambridge, 2009. 21174
Vandaele, A., Hermans, C., Simon, P., Van Roozendael, M., Guilmot, J., Carleer, M., and Colin, R.: Fourier Transform Measurement of NO_2 Absorption Cross-sections in the Visible Range at Room Temperature, J. Atmos. Chem., 25, 289–305, 1996. 21174
Western, C.: PGOPHER: a Program for Simulating Rotational Structure, Available: University of Bristol, http://pgopher.chm.bris.ac.uk, last access: September 2009. 21174
Zilitinkevich, S. S.: On the computation of the basic parameters of the interaction between the atmosphere and the ocean., Tellus, 21, 17–24, 1969. 21171

Table 1. Assumptions used to convert mass per gramme into mass per m^2.

Species	Minimum Depth (m)	Maximum depth (m)	Average biomass (kg FW/m^2)	Average volumic mass (kg FW/m^2)	Average volume (m^3/m^2)
L. digitata	+0.5	−1.0	10	320	0.03
L. ochroleuca	0	−5.0	10	315	0.03
L. hyperborea	0	20.0	10	310	0.03
Saccharina latissima	+0.5	−2.0	10	140	0.07
Ascophyllum/Fucus (35/65)	+1.5	+6.0	8	230	0.035

Table 2. Parameters used as input into the footprint model. Note that while the roughness length varies over water, a constant value of 0.03 m was used for runs at low tide across the inter-tidal zone. All 10 sets of parameters were run for both high and low tide cases. Measurement height was 8 m.Symbols are: z_0 – surface roughness length, σ_v – transverse velocity variance, u_* – friction velocity, L – Obukhov length.

	Day				Night			
U (ms-1)	z_0 (m)	σ_v (ms-1)	u_* (ms-1)	L (m)	z_0 (m)	σ_v (ms-1)	u_* (ms-1)	L (m)
2.00	0.00100	0.40	0.20	−25	0.00100	0.40	0.15	100
4.00	0.00100	0.80	0.40	−100	0.00100	0.60	0.30	200
6.00	0.00115	1.20	0.60	−100	0.00100	0.9	0.45	300
8.00	0.00156	1.60	0.70	−100	0.00115	1.10	0.60	200
10.00	0.00204	2.00	0.80	−100	0.00156	1.30	0.70	200

Table 3. Percentage of total regional emissions visible at site.

Species	Regional	Site (10% recyc)	LP-DOAS (10% recyc)	Site (full recyc)	LP-DOAS (full recyc)
Laminaria digitata	42.5	73.2	46.8	63.4	50.1
L. hyperborea	42.3	0.0	1.3	0.2	2.5
L. ochroleuca	9.7	17.3	47.3	28.4	41.0
Saccharina latissima	3.9	2.7	2.8	3.6	4.9
Ascophyllum/Fucus (35/65)	1.7	6.8	1.8	4.32	1.5

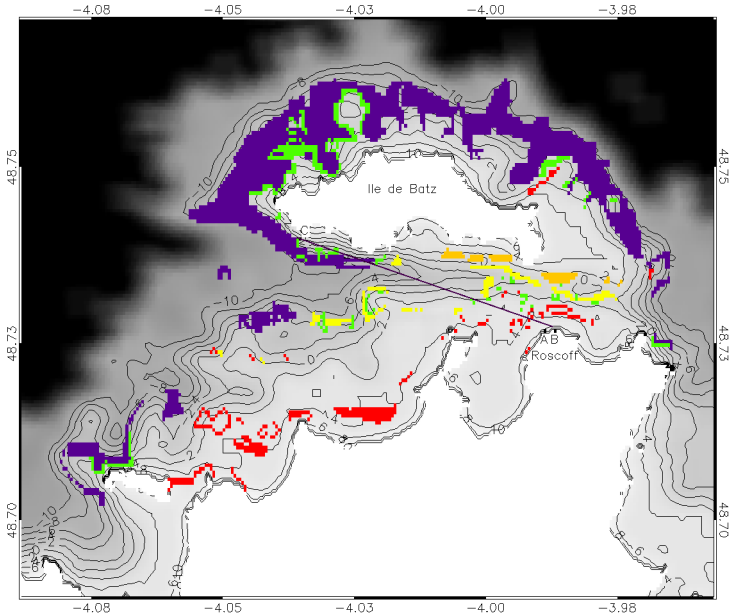

Fig. 1. Bathymetry map and algal distributions used as inputs for this modelling work. Key following key locations are marked; the main measurement site (A), the LP-DOAS telescope (B) and the LP-DOAS retroreflector (C). Seaweed species are coded as follows: *L. hyperborea* – purple, *L. digitata* – green, *L. ochroleuca* – orange, *Saccharina latissima* – yellow, *Ascophyllum/Fucus* – red.

ACPD

9, 21165–21198, 2009

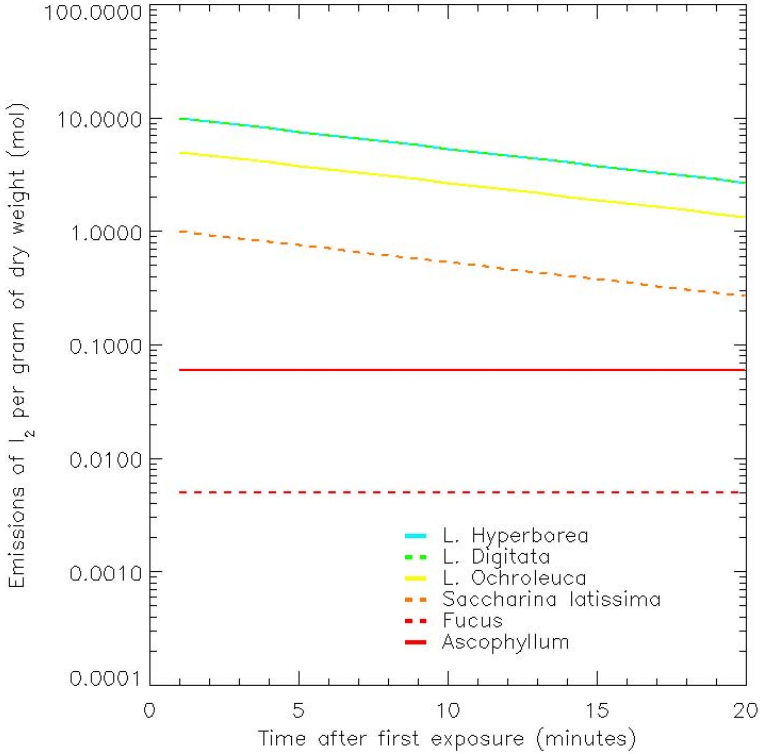

Fig. 2. The kelp bed at the Rocher du Loup, at a low tide of about 0.5 m dominated by *L. digitata* (kelp) and just above a belt of *Himanthalia elongata* (fucoid).

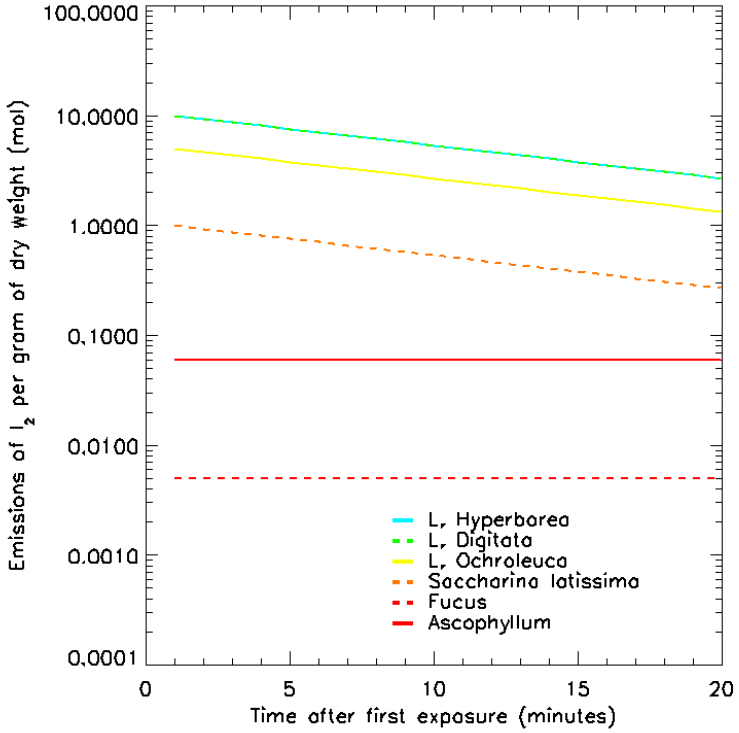

Fig. 3. Emission rates from a number of macroalgal species following exposure to an oxidising atmosphere. These data, used in this model, are taken from Ball et al. (2009).

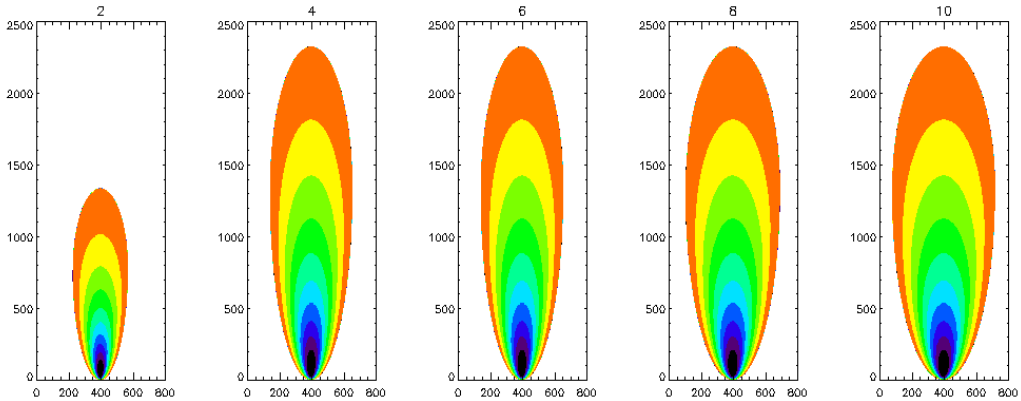

Fig. 4. Footprints used in this model, at 2, 4, 6, 8 and 10 m/s windspeed.

ACPD

9, 21165–21198, 2009

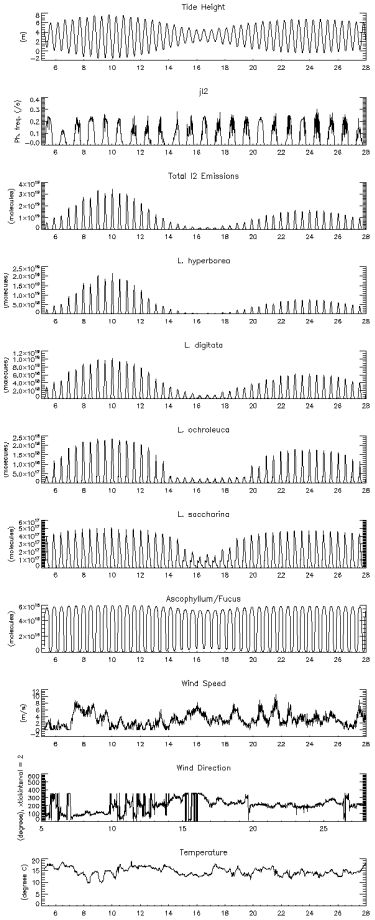

Fig. 5. Seaweed emissions, meteorolgical data and actinic flux.

ACPD

9, 21165–21198, 2009

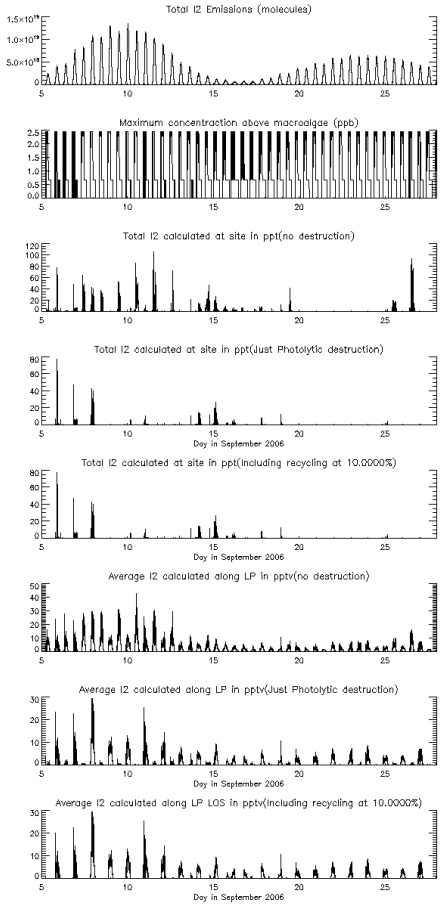

Fig. 6. Output from the model. From Top down, Regional emissions as calculated by the model, maximum calculated concentrations above macroalgal beds, site exposure based on footprint analysis calculated for no destruction processes, with photodissociation, and with photodissociation coupled with 10% recycling back into I_2.

ACPD

9, 21165–21198, 2009

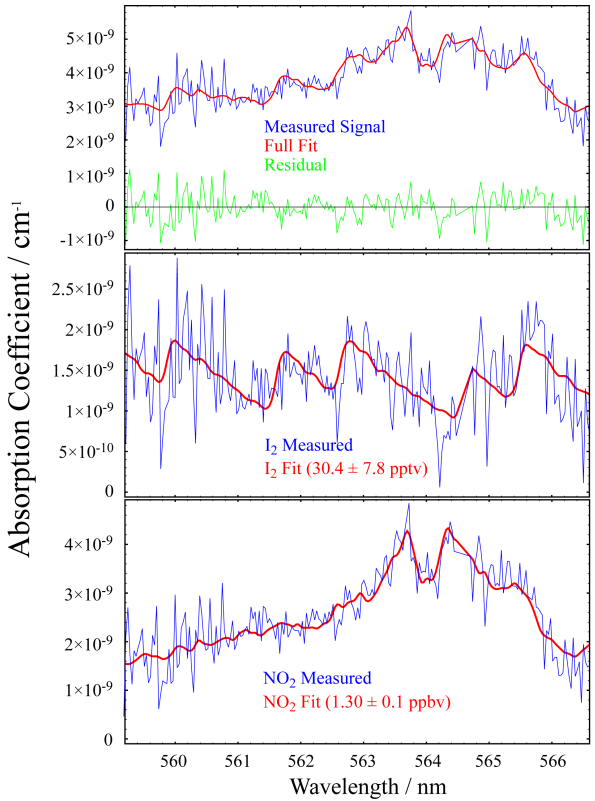

Fig. 7. An example BBCRDS spectrum recorded around 17:30 UT on 14 September 2006. The upper panel shows the measured spectrum (blue) after subtraction of the absorptions due to water vapour, O_4 and a second order polynomial accounting for the unstructured absorption contributions. The red line shows a DOAS fit to the spectrum's differential structure, and the residual spectrum is shown in green. The measured (blue) and fitted (red) absorption coefficients due to I_2 and NO_2 are shown in the middle and lower panels respectively.

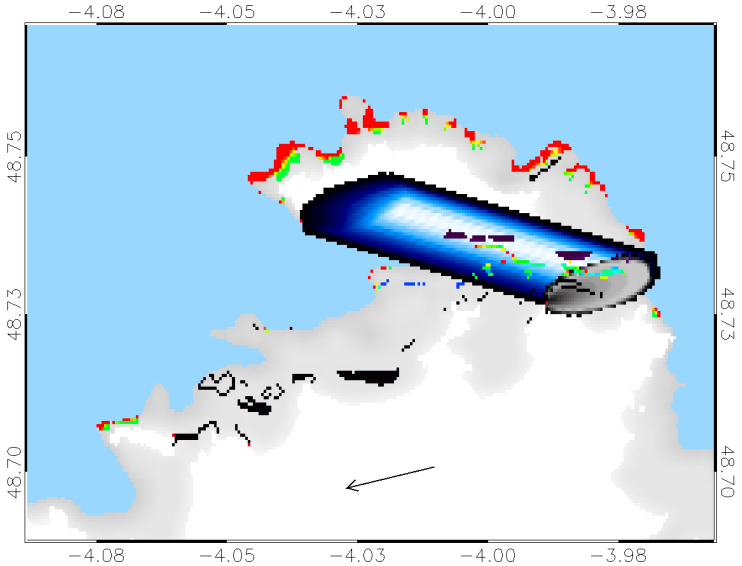

Fig. 8. Model timestep from 10:32 p.m. on 7 September 2006 during an ebb tide, one of the highest concentrations predicted at site. The windspeed and direction at this time was 5.65 m/s and 79.7 degrees respectively, with the tide 0.85 m below the datum). LP-DOAS and site footprints are shown, overlayed by estimated emissions, with red denoting an emission rate of 1×10^{17} molecules per grid square per second.

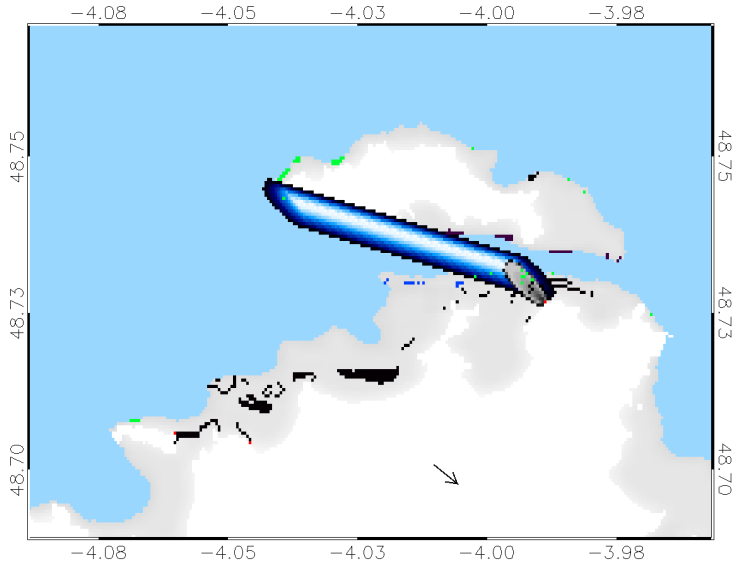

Fig. 9. Model timestep from 05:48 p.m. on 14 September 2006 during aflow tide, when the BBCRDS instrument measured significant concentrations of I_2. The windspeed and direction at this time was 1.9 m/s and 309 degrees respectively, with the tide 1.83 m above the datum). The reduction in emissions since first exposure can be seen with respect to Fig. 8.

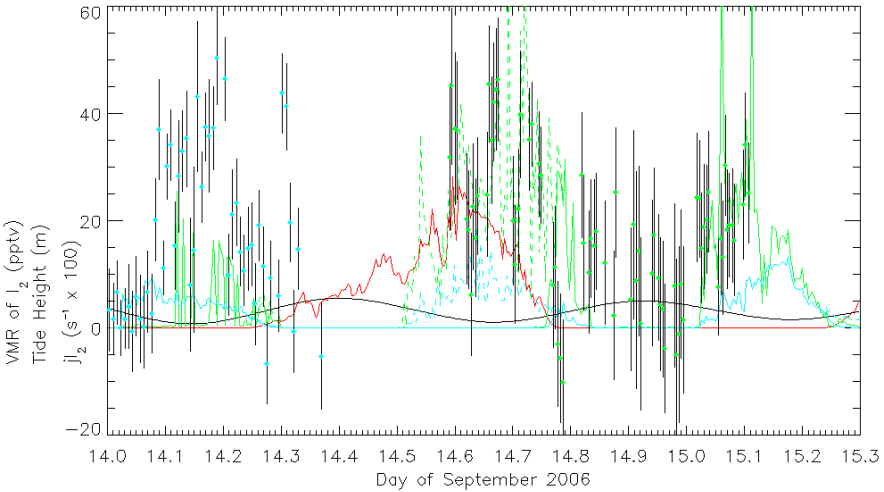

Fig. 10. Modelled and measured data from 14 September 2006. Shown are; jI_2 (red), tide height (black), modelled concentration at site and along the LP-DOAS line of site with photolytic destruction and 10% recycling (solid green and blue lines respectively), modelled concentration at site and along the LP-DOAS line of site with no destruction processes modelled (dashed green and blue lines respectively), and measurements from the LP-DOAS and BBCRDS instruments(blue and green dots respectively, with error bars).

ACPD

9, 21165–21198, 2009

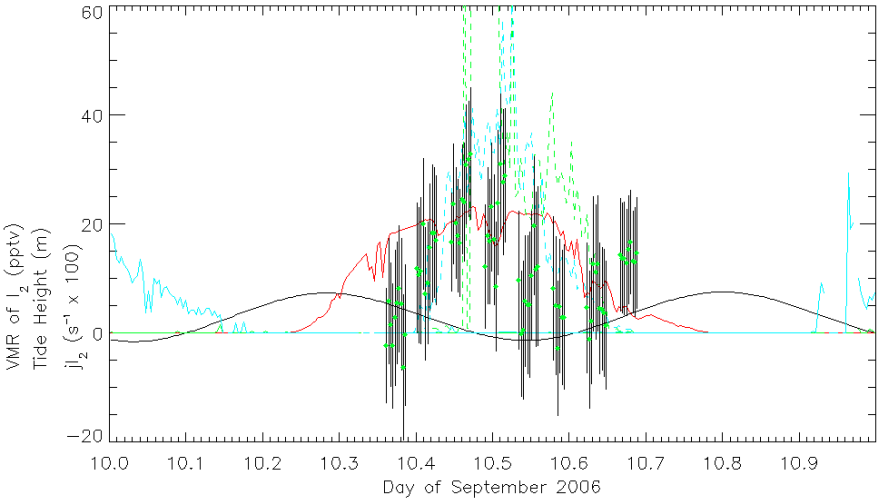

Fig. 11. Modelled and measured data from 10 September 2006. Shown are; jI_2 (red), tide height (black), modelled concentration at site and along the LP-DOAS line of site with photolytic destruction and 10% recycling (solid green and blue lines respectively), modelled concentration at site and along the LP-DOAS line of site with no destruction processes modelled (dashed green and blue lines respectively), and measurements from the LP-DOAS and BBCRDS instruments(blue and green dots respectively, with error bars).

ACPD

9, 21165–21198, 2009

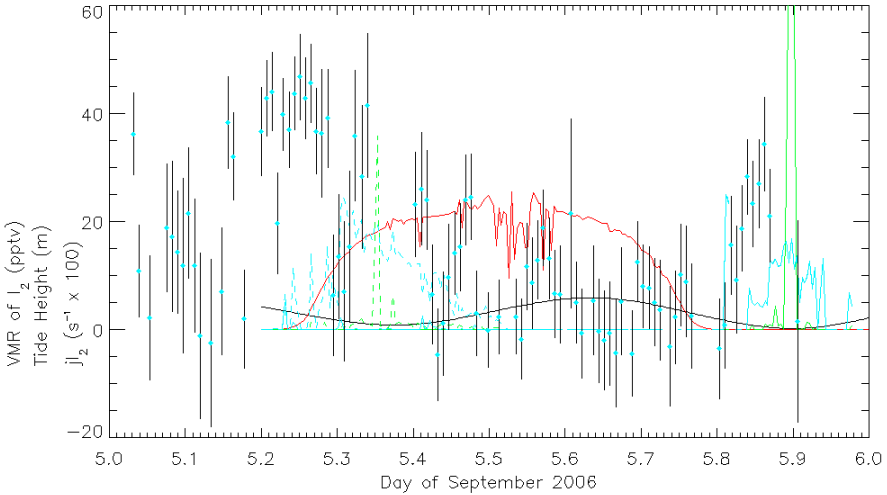

Fig. 12. Modelled and measured data from 5 September 2006. Shown are; jI_2 (red), tide height (black), modelled concentration at site and along the LP-DOAS line of site with photolytic destruction and 10% recycling (solid green and blue lines respectively), modelled concentration at site and along the LP-DOAS line of site with no destruction processes modelled (dashed green and blue lines respectively), and measurements from the LP-DOAS and BBCRDS instruments(blue and green dots respectively, with error bars).

ACPD

9, 21165–21198, 2009

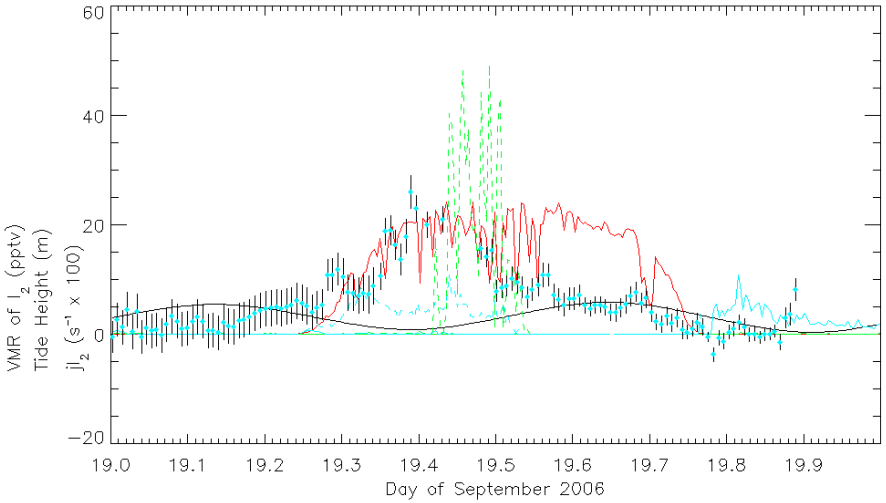

Fig. 13. Modelled and measured data from 19 September 2006. Shown are; jI_2 (red), tide height (black), modelled concentration at site and along the LP-DOAS line of site with photolytic destruction and 10% recycling (solid green and blue lines respectively), modelled concentration at site and along the LP-DOAS line of site with no destruction processes modelled (dashed green and blue lines respectively), and measurements from the LP-DOAS and BBCRDS instruments (blue and green dots respectively, with error bars).

ACPD
9, 21165–21198, 2009